J Mater Sci (2021) 56:4991–5005

Chemical routes to materials

One-pot synthesis of graphene quantum dots using humic acid and its application for copper (II) ion detection

Xiao Liu[1], Juan Han[1], Xiaodong Hou[2], Furkan Altincicek[3], Nuri Oncel[3], David Pierce[1], Xu Wu[1,*], and Julia Xiaojun Zhao[1,*]

[1] Department of Chemistry, University of North Dakota, Grand Forks, ND 58202, USA
[2] Institute for Energy Studies, University of North Dakota, Grand Forks, ND 58202, USA
[3] Department of Physics & Astrophysics, University of North Dakota, Grand Forks, ND 58202, USA

Received: 20 August 2020
Accepted: 17 November 2020
Published online: 2 December 2020

ABSTRACT

A new carbon source, humic acid, has been used in fabricating graphene quantum dots by a facial one-pot hydrothermal reaction. The morphology of the cyan emission graphene quantum dots has been characterized by high-resolution transmission electron microscopy (HRTEM). The result showed well-displayed crystalline with a lattice spacing of 0.286 nm. X-ray photoelectron spectroscopy (XPS) and Fourier-transform infrared spectroscopy (FTIR) have demonstrated the diverse functional groups on GQDs, like carboxylic groups, which will cause significant fluorescence quenching by Cu^{2+} because of the strong chelating interactions. The optical properties of GQDs were characterized by photoluminescence (PL) spectra and ultraviolet–visible (UV–Vis) spectroscopy; it showed that GQDs have an excitation-dependent fluorescence behavior and a large stoke shift with maximum excitation/emission wavelength at 360/470 nm. Furthermore, GQDs showed a good photostability by the kinetic analysis of irradiation for 1500 s and a relatively high quantum yield of 20%, which could be applied in bioimaging. Besides, the selectivity study of metal ions indicates that the GQDs could be used in Cu^{2+} detection. The linear range is from 1 to 40 μM with the limit of detection (LOD) of 0.44 μM. Overall, this work provided a simple method to produce GQDs with low-cost raw material humic acid, which could be also used in Cu^{2+} monitoring in river water.

Handling Editor: Christopher Blanford.

Address correspondence to E-mail: Xu.wu@und.edu; Julia.zhao@und.edu

https://doi.org/10.1007/s10853-020-05583-6

Introduction

Fluorescent nanomaterials, due to their unique chemical, physical and optical properties, have been proved to be pivotal tools in sensing, imaging and some other biomedical applications [1–9]. In the past few decades, a number of fluorescence nanomaterials, including organic nanomaterials and inorganic nanomaterials, have been designed and synthesized to serve as bioimaging agents instead of organic dyes. Comparing with organic dyes, the excellent photostability, bright fluorescence intensity and low synthetic cost make fluorescent nanomaterials as effective fluorescent probes for sensing and imaging of biomolecules, cells, tissues and organisms [10–22]. For example, heavy metal-based semiconducting quantum dots (QDs) such as CdSe, CdTe have been successfully produced with broad adsorption, narrow, adjustable and bright fluorescence, which allow QDs to be utilized in a number of biomedical applications [23]. However, the high cytotoxicity of their heavy metal components constrains their biological applications [24, 25]. Therefore, it is still necessary to develop more biocompatible fluorescent nanomaterials for biosensing and bioimaging.

Graphene quantum dots (GQDs), a zero-dimensional derivative from graphene, have been free from the disadvantages of high toxicity due to its intrinsic components of carbon and oxygen. Therefore, they have attracted great attention as promising fluorescent probes for their unique features such as good water solubility, excellent photoluminescence, low toxicity, biocompatibility and high resistance to photodegradation and photobleaching [26, 27]. In general, GQDs are synthesized from carbon-based materials. There are two main strategies to prepare GQDs: top-down and bottom-up methods. The top-down methods include acidic exfoliation, electrochemical oxidation and hydrothermal synthesis, which break large-size carbon-based materials, such as graphite and activated carbon, to small-size GQDs [28, 29]. Physical treatments like sonication can accelerate the formation of GQDs. The top-down methods bring oxygen-containing functional groups to the edges of GQDs, promoting the solubility and functional sites for further bioconjugation [30]. However, the harsh reaction conditions as well as their tedious purification procedures generate a lot of burden to overcome before applying them for biomedical applications. In contrast, bottom-up methods utilized the small carbon-based precursors to form GQDs [31]. A number of precursors, including glucose, citric acid, polythiophene, have been used for preparation of GQDs for different applications [32–34]. We recently developed a highly fluorescent GQD for bioimaging using glutamic acid due to its biocompatibility. Meanwhile, the bottom-up approach provides an easy pathway to dope multiple heteroatoms in GQDs to adjust their optical properties for further applications. For example, we prepared a N, S-doped GQDs using aspartic acid and cysteine as the carbon precursors and heteroatomic as the nitrogen and sulfur sources for bioimaging [35]. Dan et al. fabricated an S, N co-doped GQD by using citric acid as a carbon source and thiourea as a S and N source in a facile solvothermal route for visible light H_2 production and bioimaging [36]. Moreover, more wastes from the natural products have been also utilized for preparation of GQDs, such as rick husks, dead leaves, and biomass wastes. However, compared with the organic precursors, it is still in the very early stage to prepare GQDs from the natural wastes. Therefore, the preparation of high-quality GQDs from the cheap, nontoxic precursors is of importance and urgent, especially for large-scale production.

Humic acid is a natural carbon source of high molecular weight organic compounds, which is abundant in a broad range of raw materials such as peat, soils, black coals, dystrophic lake, sea sediments and other natural materials [37, 38]. Among all of the sources of humic acid, coal, and in particular low-rank coal like lignite or naturally oxidized lignite (leonardite), is the most abundant and commercialized source. For example, North Dakota leonardite (named after A.G. Leonard, the first director of the North Dakota Geological Survey) has the highest humic acid (up to 86% dry and ash-free basis) content among all sources worldwide [39]. In general, humic acid is considered as a by-product of biological or chemical decompositions of plant and animal residues. Thus, there are no specific structures of humic acid due to the diversity of humification pathways. It has been proposed that most humic acids have a lot of aromatic ring structures as the core structure substituted by multiple chemical reactive functional groups such as carboxyl, phenolic, aldehydes, ketones, alcoholic hydroxyls and quinones. The dominant carboxyl and phenolate groups enable

humic acid to form complexes with common cations such as Mg^{2+}, Ca^{2+}, Fe^{2+}, and Fe^{3+} to create humic colloids [40]. Comparing with graphene-based starting materials, humic acid contains the similar high conjugated sp^2 carbon hybridization domains, aromatic and benzene ring structures. Therefore, humic acid would be qualified to serve as a new carbon source to synthesize graphene quantum dots [41]. In the last few decades, the technology to extract humic acid from industrial waste and straw has provided sufficient feedstocks for the possible large-scale production of GQDs [42].

In this work, we have successfully fabricated a highly fluorescent GQD using lignite-derived humic acid as the cost-effective precursor. The preparation was conducted by the hydrothermal treatment of humic acid in a basic solution with autoclave at 200 °C for 12 h. The characterization of GQDs showed that a plentiful of functional groups were presented on GQDs. Fluorescence and UV–Vis spectroscopy analysis showed that GQDs demonstrated bright blue fluorescence with quantum yield of ca. 20%, and the fluorescence emission was excitation dependent. Comparing with other precursors used to prepare GQDs with the bottom-up method, this work started with lignite-derived humic acid as a precursor, which would largely reduce the cost for scale-up production. Finally, we found that the fluorescence GQDs showed fluorescence quench with the addition of copper ions (Cu^{2+}). With the optimal detection conditions, the GQDs could detect Cu^{2+} in the range of 1 μM–40 μM with the limit of detection of 0.44 μM. The sensing assay was also successfully presented to be used for the detection of Cu^{2+} in river water, which demonstrates potential usage in environmental monitoring of the proposed GQDs.

Experimental

Chemicals

Humic acid was extracted and purified from North Dakota lignite by the Institute for Energy Studies. Ammonium hydroxide (NH_4OH, 28.0%–30.0%), 4-(2-hydroxyethyl)-1-piperazineethanesulfonic acid (HEPES), copper sulfate, and sodium hydroxide were obtained from Sigma-Aldrich. Sterile syringe filter (0.45 μm cellulose acetate) was provided by ThermoFisher Scientific. High-purity liquid argon and ultra-high-purity helium gas obtained from Airgas were used in the ICP-MS measurements. The 100 ppm Cu, Sc, and Rh stock solutions provided from Inorganic Ventures were used during the ICP-MS measurements. All chemicals were of analytical grade unless specified. All buffer solutions were prepared using ultrapure water (18 MΩ cm) from a Millipore Milli-Q water purification system.

Synthesis of GQDs

The GQDs were produced by a simple hydrothermal method. Briefly, 10.0 mg of humic acid was dispersed in 8.0 mL 0.28%–0.30% (0.15 M) aqueous ammonium hydroxide solution first, and then, the pH was optimized by 1.0 mol/L NaOH solution to reach a final volume of 10.0 mL and a final pH about 10. The black solution was sonicated and transferred into a 25.0-mL Teflon-lined stainless-steel autoclave. The synthesis process was conducted in a 200 °C oven for 12 h. After the autoclave was cooled down to room temperature, the color of the solution turned to brown, indicating the formation of GQDs. Finally, the solution was centrifuged at 10,000 rpm for 20 min to remove the large particles. The supernatant was further dialyzed in a dialysis bag (molecular weight cutoff = 10,000) for 48 h against water to purify the produced GQDs. Three portions of produced GQDs were collected in the evaporation dish to remove water and adjust the final stock solution to 2.0 mg/mL.

Characterization of GQDs

A JEOL JEM-2100 high-resolution transmission electron microscope (HRTEM) (JEOL Ltd., Tokyo, Japan) was used to take images of GQDs at 200 kV. A Hitachi 7500 Transmission Electron Microscope (Hitachi, Tokyo, Japan) was used to take images of GQDs at 80 kV. The hydrodynamic diameter of GQDs was recorded from Zetasizer Nano ZS (Malvern, Worcestershire, UK). A PerkinElmer Lambda 1050 UV/VIS/NIR spectrometer (PerkinElmer, Santa Clara, CA, USA) was used to obtain the absorption spectra of GQDs. Fluorescence measurements were taken with a RF-6000 fluorophotometer (SHIMADZU, Kyoto, Japan). The excitation wavelength was set to be 360 nm, and the emission was recorded from 380 to 700 nm. The fluorescence intensity at 470 nm was selected to evaluate the performance for

copper ions detection. Both the widths of excitation and emission slits were 10.0 nm. All the experiments were carried out at 25 °C. A FTIR Spectrum ATR iD5 spectrometer (ThermoFisher Scientific, Waltham, UK) was used to collect the Fourier transform infrared (FTIR) spectra of GQDs. The X-ray photoelectron spectroscopy (XPS) measurements were taken on a PHI-5400 X-ray photoelectron spectrometer (ULVAC-PHI, Japan) with 10^{-10} Torr base pressure. The Al Kα (1486.6 eV) X-ray radiation was used as the X-ray source, powered at 300 W for excitation. An X-ray diffraction (XRD) profile was recorded on a Smartlab-3KW X-ray diffractometer (Rigaku, Tokyo, Japan) with CuKα as the X-ray radiation source at 40 kV and 44 mA. Teflon-lined hydrothermal synthesis autoclave reactor (APT, RI, USA) and PTFE-lined vessel (25 mL) were used to synthesize GQDs. Symphony vacuum oven (VWR, PA, USA) was utilized to heat up the reaction system to 200 °C. An iCAP Qc ICP-MS (Thermo Scientific, Bremen, Germany) combined with a 4-channel 12-roller peristaltic pump and a Teledyne CETAC ASX560 autosampler (Omaha, NE) were used to determine the concentrations of Cu^{2+} in Red River water samples. The THERMO-4AREV (Thermo Scientific) standard was run daily to optimize the ICP-MS with maximum ^{59}Co, ^{238}U and minimum $^{140}Ce/^{140}Ce$ oxide signal in the kinetic energy discrimination. The ICP-MS measurements of Cu^{2+} concentrations were collected using the Qtegra™ software (version 2.8.2944.202). The isotopes of ^{45}Sc and ^{103}Rh were used as internal standard in the ICP-MS measurements.

Stability of GQDs over pH and photostability

1.0 mL of 1.0 mg/mL GQDs solution was incubated in different pH buffers, ranging from 1 to 12 for 1 h. Then, the fluorescence intensity of the GQDs solution at different pHs was recorded. In order to investigate the photostability of GQDs, a time-based fluorescence collection was performed with a 1.0 mL of GQDs solution (1.0 mg/mL) for 1500 s. FITC was used as a control group.

Quantum yield (QY) measurement

Quinine sulfate in 0.1 M H_2SO_4 (QY = 0.54 at 360 nm) was chosen as a standard for quantum yield measurement. The quantum yield of GQDs was calculated according to the following formula:

$$\Phi_x = \Phi_{st}\left(\frac{\mathrm{Grad}_x}{\mathrm{Grad}_{st}}\right)\left(\frac{\eta_x^2}{\eta_{st}^2}\right)$$

Here, Φ_x is the quantum yield of GQDs. Grad is the gradient from the plot of integrated fluorescence intensity *vs* absorbance, and η is the refractive index of the solvent (1.33 for water). The subscript "st" stands for the standard of quinine sulfate and "x" stands for GQDs. In order to minimize reabsorption effects, absorbances of the samples were kept under 0.1 at the excitation wavelength (360 nm).

Copper (II) ion detection procedure

In order to investigate the quenching ability of Cu^{2+} on GQDs, we incubated the 1.0 mL of the final concentration of 0.4 mg/mL GQDs with different concentrations of Cu^{2+} for 12 h. The fluorescence intensity at 470 nm with excitation of 360 nm was recorded for each concentration. The concentration of Cu^{2+} ranged from 0 to 300 μM.

Selectivity investigation

In order to investigate the selectivity of GQDs on different metal ions, a final volume of 1.0 mL of 0.4 mg/mL GQDs solution was incubated with different metal ions, including, Ni^{2+}, Ca^{2+}, Co^{2+}, Cd^{2+}, Mg^{2+}, Cu^{2+}, Zn^{2+}, Fe^{3+}, Mn^{2+}, Na^{+}, K^{+}, Ag^{+}, and Pb^{2+}. The concentration of each metal ion was 20 μM. All the fluorescence intensities at 470 nm were recorded at the excitation wavelength of 360 nm.

Results and discussion

Design and preparation of the highly fluorescent GQDs

A simple bottom-up method was developed to fabricate GQDs from humic acid by a one-pot hydrothermal reaction. The formation of GQDs is illustrated in Scheme 1. First, in order to enhance the solubility of humic acid in the aqueous solution, the pH of the solution with 10 mM humic acid was adjusted to 10 by ammonia hydroxide. During this process, humic acid was dissolved completely with ultrasonication and a dark black solution was

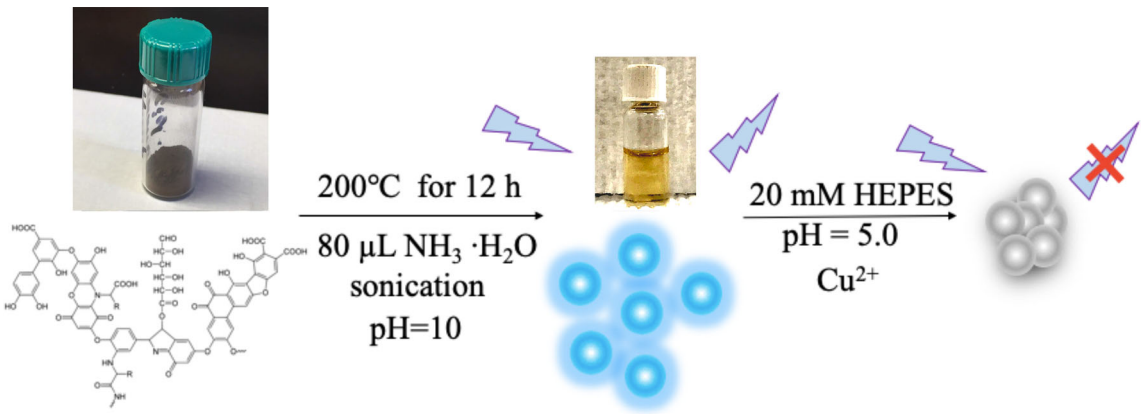

Scheme 1 Schematic illustration of the formation of GQDs and its application for Cu^{2+} detection.

obtained. Afterward, an aliquot of 10.0 mL of the above solution was transferred into an autoclave and put into an oven at 200 °C for 12 h. After the purification, the highly fluorescent GQDs were obtained. Due to the abundant coverage of carboxyl groups on the prepared GQDs, we proposed that the formed GQDs might have specific response to Cu^{2+} (Scheme 1). The uniqueness of this high brightness cyan emission GQDs is the starting material together with simple preparation procedures. Compared with the starting materials in Table 1, the carbon source of this project is humic acid, which could be obtained from natural products' waste. Therefore, this GQD with high quality could be obtained by a low-cost and environmental-friendly process, especially for large-scale production. The humic acid used by this method could be obtained locally from low-rank coal called lignite (North Dakota leonardite), which contains high mass percent of humic acid (up to 86% dry and ash-free basis) content. Therefore, this method could provide a potential pathway to utilize the abundant carbon source for commercial production of GQDs in the future.

Characterization of graphene quantum dots

To characterize the morphology and diameter of the GQDs, a high-resolution TEM was performed (Fig. 1). The GQDs showed a spherical shape with good mono-dispersity, whose diameter was in the range of 3–10 nm. Meanwhile, the lattice spacing of GQDs was measured to be about 0.286 nm, indicating the characteristic structure of the graphitic carbon [49]. The hydrodynamic diameter measured by DLS was 6.5 ± 2.3 nM (Fig. 1d), which was slightly larger than that measured from TEM.

The X-ray diffraction (XRD) was also performed to characterize the graphitic nature of the GQDs. As shown in Fig. 2a, there was a broad peak centered at $2\theta = 25°$, corresponding to an interlayer spacing of 0.286 nm, and the result is smaller than that of graphite (002), which is caused by the bending of interlayers [50]. To identify the formation and surface

Table 1 Comparison of the proposed methods with other methods

Methods	Subclassification	Starting material	Size (nm)	Color	Yield %	Reference
Top-down	Acidic oxidation	Carbon Black	18	Yellow	9	[43]
	Hydrothermal	GO	5–13	Blue	5	[44]
	Microwave	GO	2–7	Greenish yellow	11.7	[45]
	Solvothermal	GO	3–5	Blue to green	1.6	[46]
Bottom-up	Microwave-assisted hydrothermal	Glucose	~ 5	Blue	15	[47]
	Precursor pyrolysis	Citric acid	0.8–1.8	Blue	3.6	[48]
	Hydrothermal	Humic acid	3–10	Cyan	20	This work

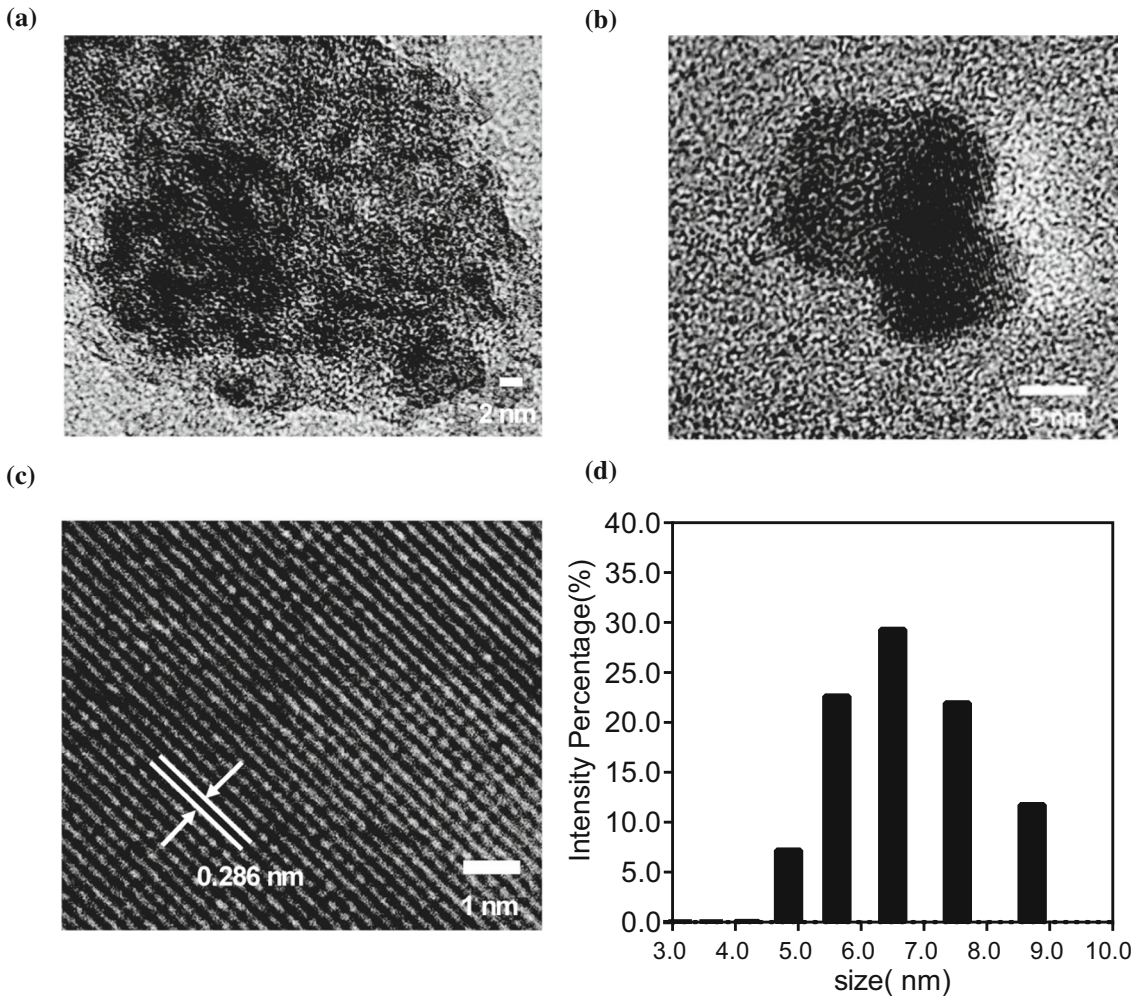

Figure 1 **a**–**b** TEM images of the GQDs. **c** HRTEM image of the GQDs (0.286 nm). **d** The size distribution of the GQDs detected by DLS.

functional groups of GQDs, X-ray photoelectron spectroscopy (XPS) and FTIR were conducted. The results from XPS showed two main peaks at 285.25 eV, 532.5 eV, which were attributed to C 1 s, O 1 s, respectively (Fig. 2b). The atomic percentage of the carbon and oxygen was calculated to be about 80% and 20%, respectively, which were the main elements in the prepared GQDs. The C 1 s spectrum of GQDs (Fig. 2c) showed five peaks at 284.2 eV, 284.9 eV, 286.2 eV, 288. 2 eV, and 288.9 eV, indicating the presence of C = C, C–C/C–H, C–OH, C = O, and –COOH, respectively. All these data from XPS analyses suggested that the C and O atoms were the major components of GQDs synthesized from humic acid. FTIR was used to demonstrate the existence of various functional groups on GQDs. As shown in Fig. 2d, the peaks at 1250 cm^{-1} and 1400 cm^{-1} suggested the presence of the C–O–C and N–H stretching in graphite structure. The presence of hydroxyl groups was proved by the broad peak area at 2970 cm^{-1}, and the presence of carboxyl groups was showed in the sharp peak at 1600 cm^{-1}. Besides the carbon-related functional groups, the amine N–H functional group showed stretching vibrations of amine N–H at 3000–3500 cm^{-1}. These functional groups on GQDs provided the potential reaction sites for further modification.

Fluorescent properties of the GQDs

In addition, we investigated the fluorescent properties of the GQDs using fluorescence spectrometer. Under the irradiation of 365-nm UV light, the GQDs showed strong cyan fluorescence compared with

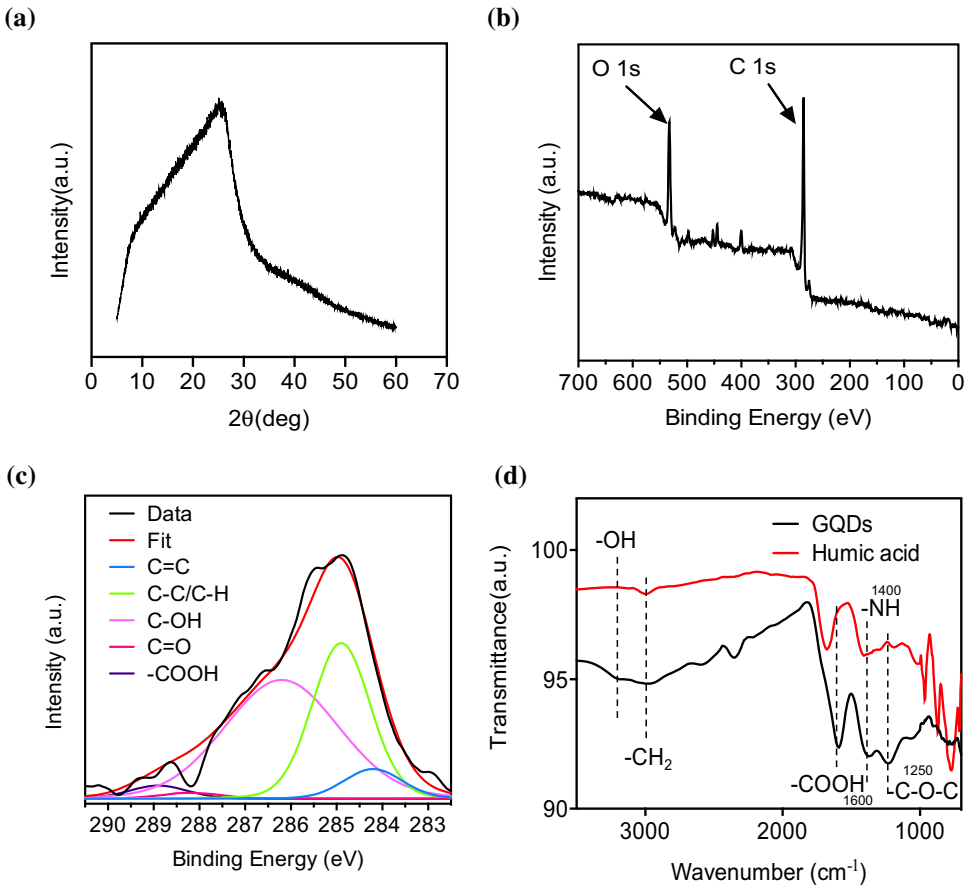

Figure 2 **a** XRD patterns of the GQDs. **b** Survey XPS spectra of the GQDs. **c** High-resolution C 1 s spectra of the GQDs. **d** The FTIR spectra of the GQDs and humic acid.

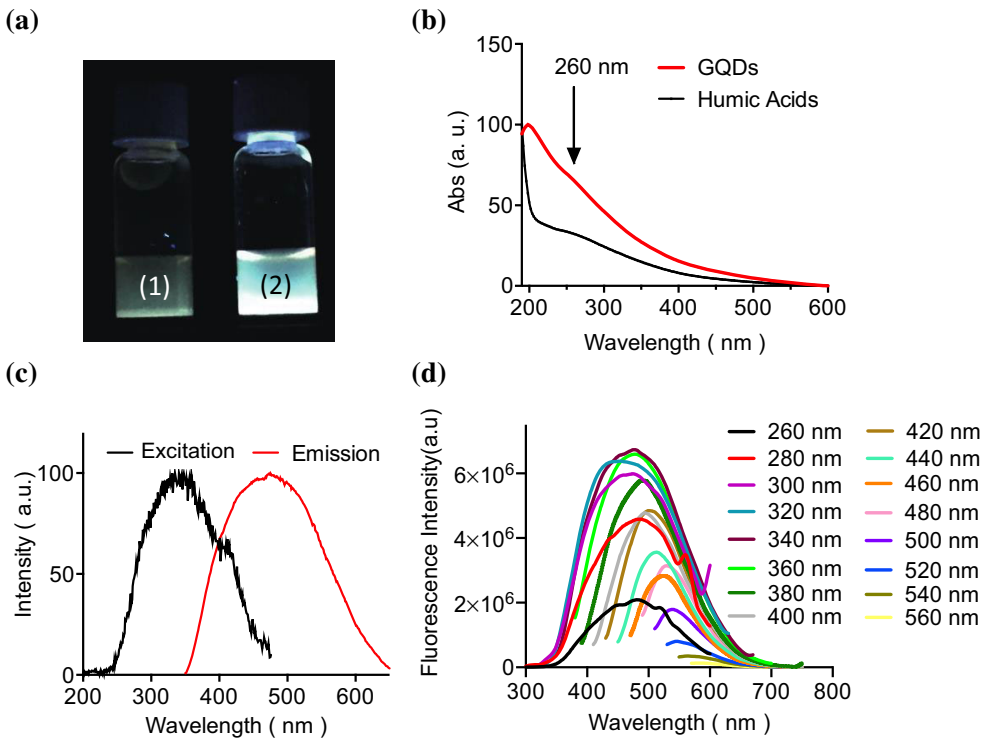

Figure 3 **a** Photographs of humic acid (1) and GQDs (2) excited under 365 nm UV light. **b** UV–Vis absorption spectrum of humic acid (black) and GQDs (red). **c** The excitation and emission spectra of GQDs. λ_{ex} = 360 nm; λ_{em} = 470 nm. **d** Fluorescence emission spectra of GQDs when the excitation wavelength increased from 260 to 560 nm.

humic acid (Fig. 3a), indicating the formation of the fluorescent GQDs. As shown in Fig. 3b, the UV–Vis absorption spectrum of the GQD aqueous solution exhibited a typically optical absorption in the ultraviolet (UV) region with a long tail expanding into the visible range. There is no obvious peak except the peak near 260 nm, which is corresponding to a π-to-π* transition of aromatic C = C bonds. In contrast, there is no obvious absorption peak for humic acid. The excitation and emission spectra of GQDs are measured and demonstrated in Fig. 3c. The strongest fluorescence emission at 470 nm was obtained when the excitation wavelength was set to 360 nm. In consistent with other similar graphene quantum dots or carbon nanodots, the developed GQDs here also showed excitation-dependent emission (Fig. 3d). When the excitation wavelength increased from 260 to 560 nm, the emission wavelength increased from 440 to 590 nm.

Photostability and pH effect

To be used for bioimaging and biosensing, the photostability and pH effect of GQDs were investigated. Using fluorescein (FITC) as a control, GQDs showed a superior photostability. It was observed that no photobleaching appeared at a long irradiation period of 1500 s (Fig. 4a). Furthermore, we investigated the effect of pH on the fluorescence of GQDs. As shown in Fig. 4b, the fluorescence intensity of GQDs significantly gradually increased when the pH of the GQDs solution increased from 1.00 to 6.00. Between pH ranges of 6.00–10.00, the fluorescence intensity of GQDs showed negligible changes, indicating the excellent stability of GQDs in this range. The GQDs are promising for biomedical applications because this pH range covers most of the physiological environment. Under strong basic condition from pH 10 to pH 12, the fluorescence intensity declined.

Fluorescence stability of GQDs on metal ions

From screening the effect of metal ions on the fluorescence of GQDs, we found a significant fluorescence quenching effect of Cu^{2+}on the GQDs. As shown in Fig. 5, a series of different metal ions were tested at the concentration of 20 μM. The results showed that the addition of Cu^{2+} significantly decreased the fluorescence intensity of GQDs, while other metal ions had no or slightly impact on the fluorescence of GQDs, which could be explained by Irving–Williams series [51]. Therefore, the developed GQDs could be used for monitoring the concentration of Cu^{2+}.

Feasibility and characteristic investigation of Cu^{2+} detection

In order to give the approval to the feasibility, we investigated the fluorescence intensity response of GQDs before and after the addition of Cu^{2+}. As shown in Fig. 6a, the fluorescence intensity of GQDs decreased by about 71% in the presence of 300 μM Cu^{2+}. Thus, GQDs could be used as a fluorescent sensing probe for Cu^{2+} detection. Figure 6a shows a lower fluorescence intensity of GQDs corresponding to a higher Cu^{2+} concentration. Besides, the TEM images of the same samples of GQDs before and after the addition of Cu^{2+} are shown in Fig. 6b and (c),

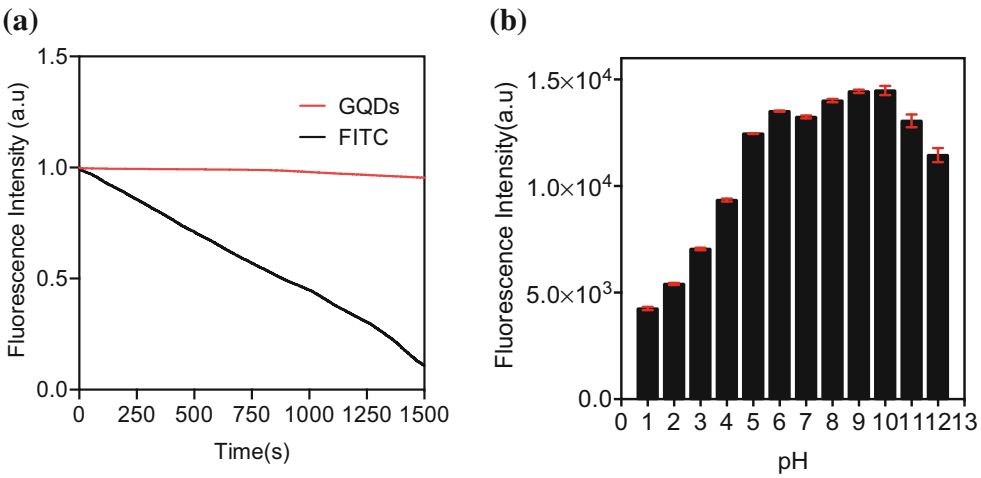

Figure 4 **a** Photostability of GQDs. **b** Effect of pH on the fluorescence intensity of GQDs.

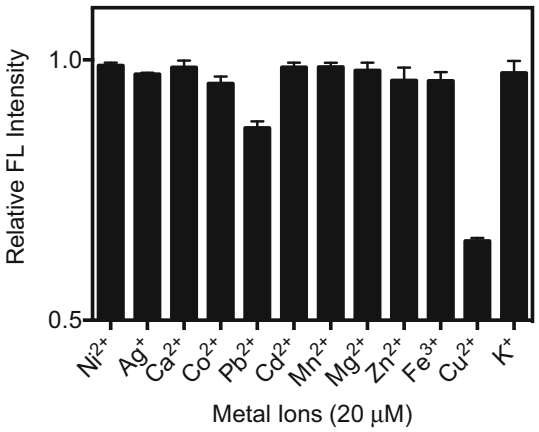

Figure 5 Effects of different ions (20 μM) on the fluorescence intensity difference of graphene quantum dots.

compared with the TEM images of GQDs in the absence(b) or presence(c) of Cu^{2+}, and GQDs were significantly aggregated in the presence of Cu^{2+} (Fig. 6c), which confirmed the proposed theory of aggregation-induced fluorescence quenching in Scheme 1. On the other hand, we also further strengthen the conclusion by monitoring the absorption spectrum of GQDs with or without the treatment of Cu^{2+}. The result is included as Fig. 6d. For the spectrum of GQDs, there is a peak at 260 nm, which belongs to the absorption peak of the fluorescent GQDs. In the spectrum of GQDs added with Cu^{2+}, no obvious peak near 260 nm was observed. Therefore, in the presence of Cu^{2+}, the aggregation of GQDs occurred corresponding to the decreased absorption peak and elevated baseline, which directly affect the fluorescence properties.

Detection of Cu^{2+}

Copper, as a transition metal, is involved in various physiological functions in biological activities, especially in cell generation and enzymatic processes [52–56]. However, copper exhibits high toxicity if over-ingested. For example, through the food chain, it will be a direct reason to cause multiple serious neurodegenerative diseases, such as Wilson and Parkinson's. Therefore, copper pollution has been

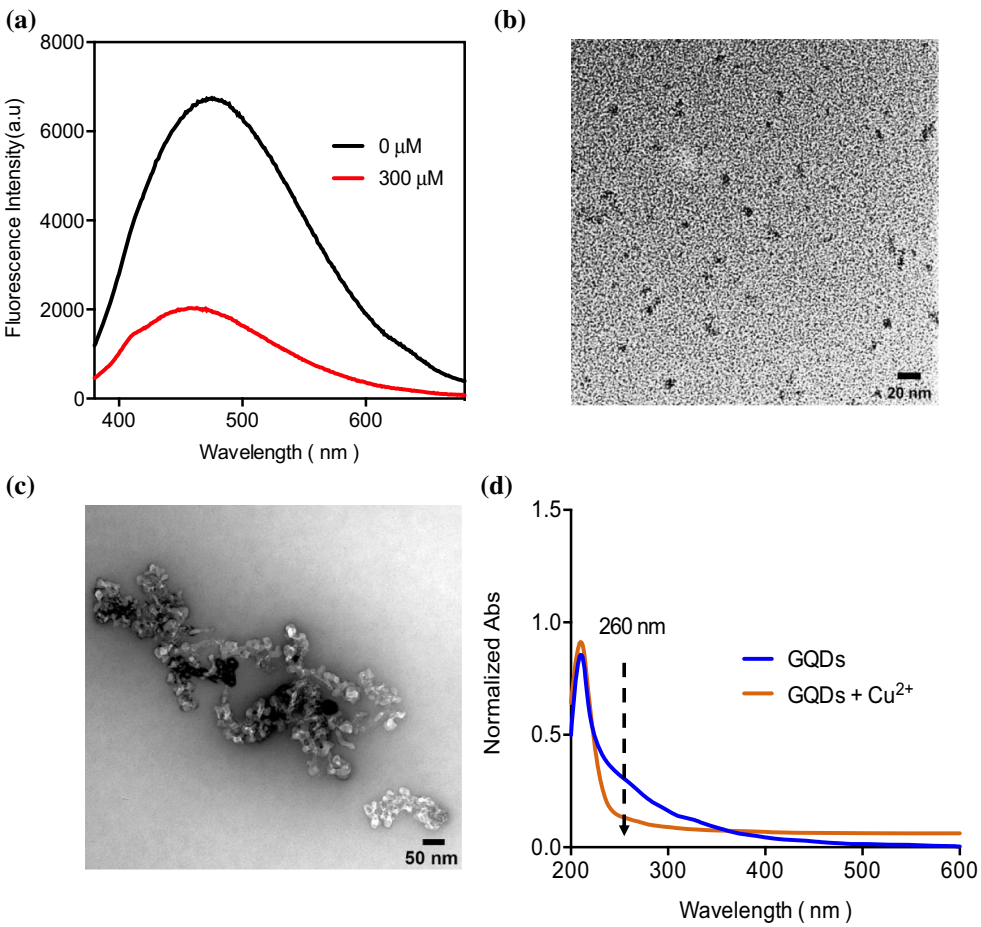

Figure 6 **a** Fluorescence spectra of GQDs incubation with two different concentrations of Cu^{2+} in 20 mM HEPES (pH 5.0). TEM images of the GQDs in the absence **b** or presence **c** of Cu^{2+} (300 μM). **d** UV–Vis absorption spectra of GQDs + Cu^{2+} (Orange) and GQDs (blue).

considered as a serious safety issue due to its wide and long-term effect. Fast and sensitive detection of copper ions in river lake and other nature resources is highly significant. The mechanism of this GQD-based sensing system is based on efficient chelating interactions between Cu(II) and carboxylic groups on the nanoparticles, which causes a significant fluorescence quenching. This could be explained by Irving–Williams series. Comparing with other transition metals, Cu^{2+} tends to form more stable bonding interactions with the abundant carboxylic groups as electron donors on the GQDs, which would cause aggregation accompanied with self-fluorescence quenching. It has been reported that carboxylic functional group-modified semiconducting polymer nanoparticles could also be quenched by Cu^{2+} through the same mechanism of strong interaction-induced self-quenching [57]. In order to optimize the reaction conditions for detecting Cu^{2+}, the effect of the concentration of GQDs, the pH, and the reaction time was investigated to obtain the largest signal-to-noise ratio. As shown in Fig. 7a, a series of concentrations of GQDs were incubated with 50 μM Cu^{2+} in 20 mM HEPES at pH 5.0 overnight, and the fluorescence intensity of the above solutions was recorded and designated as F. As a control, the same concentration of GQD solutions without Cu^{2+} in 20 mM HEPES was kept stirring overnight. The fluorescence intensities of these control groups were defined as F_0. The corresponding ratios between F and F_0 reached the minimum value at the concentration of 0.40 mg/mL of GQDs, indicating the optimal concentration of GQDs for sensing Cu^{2+}. Therefore, we utilized the concentration GQDs at 0.40 mg/mL for the following experiments.

Additionally, the optimal pH and reaction time were investigated to obtain the best performance of the sensor. As shown in Fig. 7b, with the increase in pH from 5.0 to 9.0, the ratio of F to F_0 increased significantly, which indicated that the quenching efficiency of Cu^{2+} was declined. To obtain the best analytical performance, pH 5.0 was chosen as the optimal pH of the reaction solution. Furthermore, the reaction time is critical because the interaction between GQDs and Cu^{2+} needs sufficient reaction time to complete. Therefore, we investigated the impact of reaction on the fluorescence quenching ability of Cu^{2+} to GQDs. As shown in Fig. 7c, the

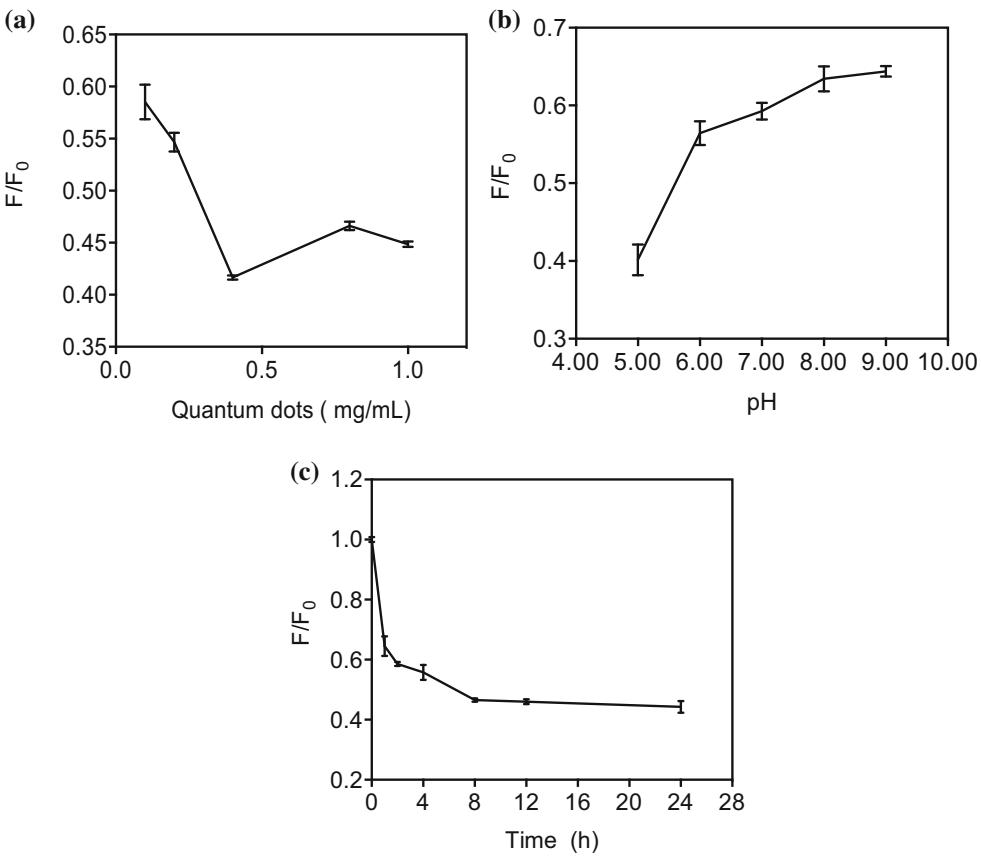

Figure 7 **a** The effect of concentration of GQDs on the sensitivity of the sensor. **b** The effect of pH on the sensitivity of the sensor. **c** The effect of reaction time on the sensitivity of the sensor. F and F_0 refer to the fluorescence intensity of GQDs with and without the addition of Cu^{2+}, respectively. λ_{ex} = 360 nm, λ_{em} = 470 nm.

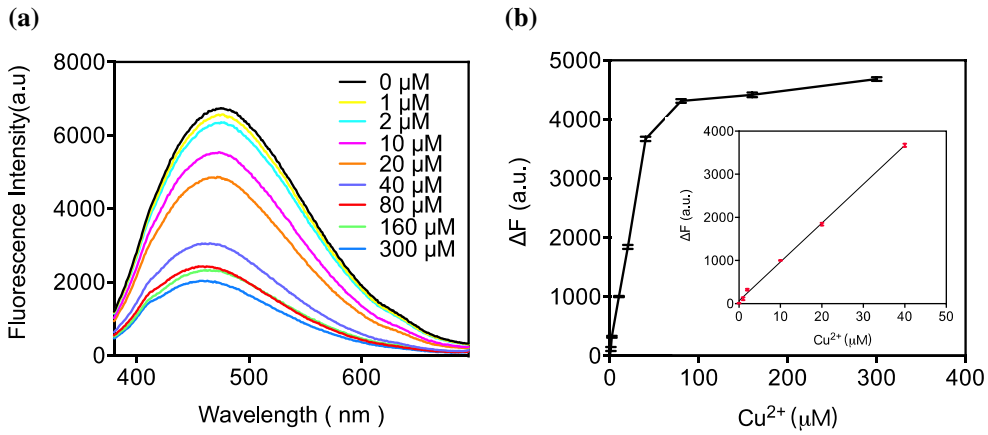

Figure 8 **a** Fluorescence spectra of GQDs incubation with different concentrations of Cu^{2+} in 20 mM HEPES (pH 5.0). **b**. The plot of the fluorescence quenching values ΔF vs the concentrations of Cu^{2+}. The inset graph in **(b)** shows the calibration curve of the sensor for Cu^{2+} detection. λ_{ex} = 360 nm, λ_{em} = 470 nm. The error bar represents standard deviation of the mean, n = 3 for each concentration.

ratio of F to F0 decreased in the first 8 h quickly and reached the plateau after 12 h. Consequently, the reaction time was optimized to 12 h.

To analyze the sensitivity of the GQDs toward Cu^{2+}, under the optimized reaction conditions (0.40 mg/mL in 20 mM HEPES buffer, pH = 5.0, 12 h reaction time), different concentrations of Cu^{2+} were incubated with GQDs and followed by the measurements of the fluorescence spectra. As shown in Fig. 8a, the fluorescence intensity of GQDs decreased as the concentration of Cu^{2+} increased from 0 μM to 300 μM. Figure 8b shows the relationship between the fluorescence quenching value $\Delta F = F_0 - F$ (F0 and F represent the fluorescence intensity of GQDs in the absence and presence of Cu^{2+}, respectively) and the concentration of Cu^{2+}. The curve showed that the dynamic range of the sensor was from 0 to 300 μM, with a linear range between 0 to 40 μM (inset of Fig. 8b). The calibration curve demonstrated a regression equation of $\Delta F = 90.21C + 63.59$ with a correlation coefficient of 0.9984, where C stands for the concentration of Cu^{2+}. The limit of detection (LOD) for the detection of Cu^{2+} was calculated to be 0.44 μM based on the slope of Eq. ($3\sigma/s$), where σ is the standard deviation of three blank signals and s is the slope of the calibration curve. We added Table 2 as shown below to compared with other methods [59–62]; the detection limit of GQD-based system toward Cu^{2+} is much lower than the above-reported methods (Table 2), which might contribute to the carboxylic group-functionalized GQDs having better binding efficiency to the divalent Cu^{2+}. Moreover, compared with other reported systems, the sensing materials of this work were GQDs produced by humic acid, which is less expensive and easy to prepare. The LOD of this work is 0.44 μM and the linear range is from 1 to 40 μM; this LOD could ensure the feasibility to apply this sensor to monitor Cu^{2+} in drinking water, because the Environmental Protection Agency (EPA) has required the highest concentration level of Cu^{2+} in drinking water to be 20 μM [58].

Analysis of spiked sample

To validate the applicability of GQDs to be utilized for Cu^{2+} detection, river water samples were spiked with two different levels of Cu^{2+} (10 μM and 20 μM),

Table 2 Comparison of the proposed sensor with other methods

Sensing material	LOD	Linear range	Method	Reference
Au nanoparticles	20 μM	20–100 μM	Colorimetric	[59]
Silver nanoclusters	5 μM	5–150 μM	Fluorometric	[60]
AuNps-DDTC	14.9 μM	1.0–10 mM	Colorimetric	[61]
Proline, PVBC polymer	0.7 μM	5–200 μM	IAS	[62]
GQDs	0.44 μM	1–40 μM	Fluorometric	This work

Table 3 Spike recovery level of conventional ICP-MS and fluorometric methods for Cu^{2+} detection in river water ($n = 3$)

Methods	Samples	Spiked	Detected	Recovery of this method (%)
Fluorometric	River water (Red River)	10.0 μM	10.22 ± 0.99 (μM)	102 ± 9.9
	River water (Red River)	20.0 μM	18.87 ± 0.23 (μM)	94 ± 1.1
Conventional ICP-MS	River water (Red River)	10.0 μM	10.28 ± 1.78 (μM)	103 ± 17.8
	River water (Red River)	20.0 μM	20.27 ± 1.49 (μM)	102 ± 7.5

followed by detecting both fluorescence signal and conventional ICPMS signal. Red River water was obtained from Grand Forks, North Dakota, USA. The spike recovery results from these two methods are shown in Table 3. Both the fluorometric method and conventional ICPMS methods showed decent recoveries; the recoveries of all samples from fluorometric assay were 102% and 94% at these two different concentrations, respectively, indicating that this new developed GQD would be applicable to the detection of Cu^{2+} in environmental waters. Besides, comparing with conventional ICP-MS method, the fluorometric method is less cost and simpler.

Conclusions

In summary, we have developed a strong cyan emission graphene quantum dots with excellent fluorescence properties using raw materials of humic acid from an abundant source—low-rank coal lignite. The procedure was a one-pot synthesis. The fluorescence intensity of this new developed GQD showed proportional response to the concentration of Cu^{2+} due to the fluorescence quenching by the strong chelating interactions between carboxylic groups and Cu^{2+}. The analysis showed a linear range from 1 to 40 μM Cu^{2+} and a limit of detection (LOD) 0.44 μM. Moreover, the method was also used to test Cu^{2+} in river water, demonstrating its applicability in complex environment.

Acknowledgements

This work was supported by the NSF grant CHE 1709160, NSF Coorperative Agreement Award OIA-1946202 and Applied Research to Address the State's Critical Needs Initiative program of UND A&S College Image Analysis Core Facility is supported in part by NIH grant 1P20GM113123 and P20GM103442. We also acknowledge the contribution of Miss. Shuyi He for helping to edit the manuscript.

Compliance with ethical standards

Conflict of interest The author(s) declare that they have no competing interests.

References

[1] Zhu C, Yang G, Li H, DuLin DYJ (2015) Electrochemical sensors and biosensors based on nanomaterials and nanostructures. Anal Chem 87:230–249. https://doi.org/10.1021/ac5039863

[2] Hong G, Diao S, Antaris AL, Dai HJCr, (2015) Carbon nanomaterials for biological imaging and nanomedicinal therapy. Chem Rev 115:10816–10906. https://doi.org/10.1021/acs.chemrev.5b00008

[3] Liang H, Zhang X-B, Lv Y, Gong L, Wang R, Zhu X, Yang R, Tan W (2014) Functional DNA-containing nanomaterials: cellular applications in biosensing, imaging, and targeted therapy. Chem Rev 47:1891–1901. https://doi.org/10.1021/ar500078f

[4] Chen J, Wu X, Hou X, Su X, Chu Q, Fahruddin N, Zhao JX (2014) Shape-tunable hollow silica nanomaterials based on a soft-templating method and their application as a drug carrier. ACS Appl Mater Int 6:21921–21930. https://doi.org/10.1021/am507642t

[5] Kimmel DW, LeBlanc G, Meschievitz ME, Cliffel DE (2012) Electrochemical sensors and biosensors. Anal Chem 84(2):685–707. https://doi.org/10.1021/ac202878q

[6] Shi J, Votruba AR, Farokhzad OC, Langer R (2010) Nanotechnology in drug delivery and tissue engineering: from

discovery to applications. Nano Lett 10(9):3223–3230. https://doi.org/10.1021/nl102184c

[7] Blum AP, Kammeyer JK, Rush AM, Callmann CE, Hahn ME, Gianneschi NC (2015) Stimuli-responsive nanomaterials for biomedical applications. J Am Chem Soc 137(6):2140–2154. https://doi.org/10.1021/ja510147n

[8] Taylor-Pashow KML, Della Rocca J, Huxford RC, Lin W (2010) Hybrid nanomaterials for biomedical applications. Chem Commun 46(32):5832–5849. https://doi.org/10.1039/C002073G

[9] Wang J, Ma Q, Wang Y, Shen H, Yuan QJN (2017) Recent progress in biomedical applications of persistent luminescence nanoparticles. Nanoscale 9(19):6204–6218. https://doi.org/10.1039/C7NR01488K

[10] Mader HS, Kele P, Saleh SM, Wolfbeis OS (2010) Upconverting luminescent nanoparticles for use in bioconjugation and bioimaging. Curr Opin Chem Biol 14:582–596. https://doi.org/10.1016/j.cbpa.2010.08.014

[11] Zhou C, Yang S, Liu J, Yu M, Zheng JJEB (2013) Luminescent gold nanoparticles: a new class of nanoprobes for biomedical imaging. Exp Biol Med 238:1199–1209. https://doi.org/10.1177/1535370213505825

[12] Wang F, Tan WB, Zhang Y, Fan X, Wang MJN (2005) Luminescent nanomaterials for biological labelling. Nanotechnology 17(1):R1–R13. https://doi.org/10.1088/0957-4484/17/1/r01

[13] Tang F, Wang C, Wang J, Wang X, Li L (2014) Fluorescent organic nanoparticles with enhanced fluorescence by self-aggregation and their application to cellular imaging. ACS Appl Mater Int 6:18337–18343. https://doi.org/10.1021/am505776a

[14] Feldmann CJN (2011) Luminescent nanomaterials. Nanoscale 3:1947–1948. https://doi.org/10.1039/C1NR90008K

[15] Yao C, Tong Y (2012) Lanthanide ion-based luminescent nanomaterials for bioimaging. Trends Anal Chem 39:60–71. https://doi.org/10.1016/j.trac.2012.07.007

[16] Lin C-AJ, Yang T-Y, Lee C-H, Huang SH, Sperling RA, Zanella M, Li JK, Shen J-L, Wang H-H, Yeh H-I (2009) Synthesis, characterization, and bioconjugation of fluorescent gold nanoclusters toward biological labeling applications. ACS Nano 3:395–401. https://doi.org/10.1021/nn800632j

[17] Zhang M, Bai L, Shang W, Xie W, Ma H, Fu Y, Fang D, Sun H, Fan L, Han M (2012) Facile synthesis of water-soluble, highly fluorescent graphene quantum dots as a robust biological label for stem cells. J Mater Chem 22:7461–7467. https://doi.org/10.1039/C2JM16835A

[18] Feng J, Shan G, Maquieira A, Koivunen ME, Guo B, Hammock BD, Kennedy IMJAC (2003) Functionalized europium oxide nanoparticles used as a fluorescent label in an immunoassay for atrazine. Anal Chem 75:5282–5286. https://doi.org/10.1021/ac034063m

[19] Luo S, Zhang E, Su Y, Cheng T, Shi CJB (2011) A review of NIR dyes in cancer targeting and imaging. Biomaterials 32:7127–7138. https://doi.org/10.1016/j.biomaterials.2011.06.024

[20] Resch-Genger U, Grabolle M, Cavaliere-Jaricot S, Nitschke R, Nann T (2008) Quantum dots versus organic dyes as fluorescent labels. Nat Methods 5:763. https://doi.org/10.1038/nmeth.1248

[21] Kim S, Fisher B, Eisler H-J, Bawendi M (2003) Type-II quantum dots: CdTe/CdSe (core/shell) and CdSe/ZnTe (core/shell) heterostructures. J Am Chem Soc 125:11466–11467. https://doi.org/10.1021/ja0361749

[22] Lovrić J, Bazzi HS, Cuie Y, Fortin GR, Winnik FM, Maysinger D (2005) Differences in subcellular distribution and toxicity of green and red emitting CdTe quantum dots. J Mol Med 83:377–385. https://doi.org/10.1007/s00109-004-0629-x

[23] Wuister SF, Swart I, van Driel F, Hickey SG, de Mello Donegá C (2003) Highly luminescent water-soluble CdTe quantum dots. Nano Lett 3:503–507. https://doi.org/10.1021/nl034054t

[24] Michalet X, Pinaud FF, Bentolila LA, Tsay JM, Doose S, Li JJ, Sundaresan G, Wu A, Gambhir S, Weiss S (2005) Quantum dots for live cells, in vivo imaging, and diagnostics. Science 307:538–544. https://doi.org/10.1126/science.1104274

[25] Derfus AM, Chan WC, Bhatia S (2004) Probing the cytotoxicity of semiconductor quantum dots. Nano Lett 4:11–18. https://doi.org/10.1021/nl0347334

[26] Liang J, He Z, Zhang S, Huang S, Ai X, Yang H, Han HJT (2007) Study on DNA damage induced by CdSe quantum dots using nucleic acid molecular “light switches” as probe. Talanta 71:1675–1678. https://doi.org/10.1016/j.talanta.2006.07.048

[27] Liu W, Howarth M, Greytak AB, Zheng Y, Nocera DG, Ting AY, Bawendi MG (2008) Compact biocompatible quantum dots functionalized for cellular imaging. J Am Chem Soc 130:1274–1284. https://doi.org/10.1021/ja076069p

[28] Tan X, Li Y, Li X, Zhou S, Fan L, Yang SJCC (2015) Electrochemical synthesis of small-sized red fluorescent graphene quantum dots as a bioimaging platform. Chem Commun 51:2544–2546. https://doi.org/10.1039/C4CC09332A

[29] Shao T, Wang G, An X, Zhuo S, Xia Y, Zhu CJRA (2014) A reformative oxidation strategy using high concentration nitric acid for enhancing the emission performance of graphene quantum dots. RSC Adv 4:47977–47981. https://doi.org/10.1039/C4RA06935H

[30] Yao J, Larson DR, Vishwasrao HD, Zipfel WR, Webb WW (2005) Blinking and nonradiant dark fraction of water-soluble quantum dots in aqueous solution. Proc Natl Acad Sci USA 102(40):14284. https://doi.org/10.1073/pnas.0506523102

[31] Li L, Wu G, Yang G, Peng J, Zhao J, Zhu J-JJN (2013) Focusing on luminescent graphene quantum dots: current status and future perspectives. Nanoscale 5:4015–4039. https://doi.org/10.1039/C3NR33849E

[32] Tang L, Ji R, Li X, Bai G, Liu CP, Hao J, Lin J, Jiang H, Teng KS, Yang Z (2014) Deep ultraviolet to near-infrared emission and photoresponse in layered N-doped graphene quantum dots. ACS Nano 8:6312–6320. https://doi.org/10.1021/nn501796r

[33] Xuan Y, Zhang R-Y, Zhang X-S, An J, Cheng K, Li C, Hou X-L, Zhao Y-DJN (2018) Targeting N-doped graphene quantum dot with high photothermal conversion efficiency for dual-mode imaging and therapy in vitro. Nanotech 29:355101. https://doi.org/10.1088/1361-6528/aacad0

[34] Ge J, Lan M, Zhou B, Liu W, Guo L, Wang H, Jia Q, Niu G, Huang X, Zhou H (2014) A graphene quantum dot photodynamic therapy agent with high singlet oxygen generation. Nat Commun 5:1–8. https://doi.org/10.1038/ncomms5596

[35] Schroer ZS, Wu Y, Xing Y, Wu X, Liu X, Wang X, Pino OG, Zhou C, Combs C, Pu QJAANM (2019) Nitrogen–sulfur-doped graphene quantum dots with metal ion-resistance for bioimaging. ACS Appl Nano Mater 2:6858–6865. https://doi.org/10.1021/acsanm.9b01309

[36] Qu D, Sun Z, Zheng M, Li J, Zhang Y, Zhang G, Zhao H, Liu X, Xie Z (2015) Three colors emission from S, N Co-doped graphene quantum dots for visible light H2 production and bioimaging. Adv Opt Mater 3(3):360–367. https://doi.org/10.1002/adom.201400549

[37] Novak J, Kozler J, Janoš P, Čežíková J, Tokarová V, Madronová L (2001) Humic acids from coals of the North-Bohemian coal field: I. preparation and characterisation. React Funct Polym 47:101–109. https://doi.org/10.1016/S1381-5148(00)00076-6

[38] Dong Y, Wan L, Cai J, Fang Q, Chi Y, Chen G (2015) Natural carbon-based dots from humic substances. Sci Rep 5(1):10037. https://doi.org/10.1038/srep10037

[39] R. W. Youngs and C. M. Frost (1963) Proceedings of the North Dakota Academy of Science. http://ashipunov.me/journals/pndas/pndas_1963.pdf.Accessed 24 October 2020

[40] Ikeya K, Sleighter RL, Hatcher PG, Watanabe A (2015) Characterization of the chemical composition of soil humic acids using fourier transform ion cyclotron resonance mass spectrometry. Geochim Cosmochim Acta 153:169–182. https://doi.org/10.1016/j.gca.2015.01.002

[41] Shi W, Fan H, Ai S, Zhu L (2015) Preparation of fluorescent graphene quantum dots from humic acid for bioimaging application. New J Chem 39:7054–7059. https://doi.org/10.1039/C5NJ00760G

[42] Piccolo A, Spaccini R, Drosos M, Vinci G, Cozzolino V (2018) The molecular composition of humus carbon: recalcitrance and reactivity in soils. The future of soil carbon, 1st edn. Elsevier Academic Press, Cambridge, pp 87–124

[43] Dong Y, Chen C, Zheng X, Gao L, Cui Z, Yang H, Guo C, Chi Y, Li CM (2012) One-step and high yield simultaneous preparation of single- and multi-layer graphene quantum dots from CX-72 carbon black. J Mater Chem 22(18):8764–8766. https://doi.org/10.1039/C2JM30658A

[44] Pan D, Zhang J, Li Z, Wu M (2010) Hydrothermal route for cutting graphene sheets into blue-luminescent graphene quantum dots. Adv Mater 22(6):734–738. https://doi.org/10.1002/adma.200902825

[45] Li L-L, Ji J, Fei R, Wang C-Z, Lu Q, Zhang J-R, Jiang L-P, Zhu J-J (2012) A facile microwave avenue to electrochemiluminescent two-color graphene quantum dots. Adv Func Mater 22(14):2971–2979. https://doi.org/10.1002/adfm.201200166

[46] Zhu S, Zhang J, Liu X, Li B, Wang X, Tang S, Meng Q, Li Y, Shi C, Hu R, Yang B (2012) Graphene quantum dots with controllable surface oxidation, tunable fluorescence and up-conversion emission. RSC Adv 2(7):2717–2720. https://doi.org/10.1039/C2RA20182H

[47] Tang L, Ji R, Li X, Teng KS, Lau SP (2013) Size-dependent structural and optical characteristics of glucose-derived graphene quantum dots. Part Part Syst Charact 30(6):523–531. https://doi.org/10.1002/ppsc.201200131

[48] Hong G-L, Zhao H-L, Deng H-H, Yang H-J, Peng H-P, Liu Y-H, Chen W (2018) Fabrication of ultra-small monolayer graphene quantum dots by pyrolysis of trisodium citrate for fluorescent cell imaging. Int J Nanomed 13:4807–4815. https://doi.org/10.2147/IJN.S168570

[49] Obeng Y (2009) Graphene and emerging materials for post-CMOS applications ECS transactions. Electrochemical Society, Pennington

[50] Matsuura D, Kizuka T (2012) Structures of graphene/cobalt interfaces in cobalt-encapsulated carbon nanocapsules. J Nanomater 2012:843516. https://doi.org/10.1155/2012/843516

[51] Atkins P, Overton T, Rourke J, Weller M, Armstrong F (2009) Shriver and atkins' inorganic chemistry, 5th edn. OUP Oxford, New York

[52] DiDonato M, Sarkar B (1997) Copper transport and its alterations in Menkes and Wilson diseases. Biochimica et Biophysica Acta (BBA) - Mol Basis Dis 1360:3–16

[53] Tapiero H, Townsend DM, Tew KD (2003) Trace elements in human physiology and pathology. Copp Biomed Pharmacother 57:386–398. https://doi.org/10.1016/S0753-3322(03)00012-X

[54] Hiroko K, Chie F, Wattanaporn B (2012) Inherited copper transport disorders: biochemical mechanisms, diagnosis, and treatment. Curr Drug Metab 13:237–250. https://doi.org/10.2174/138920012799320455

[55] Bandmann O, Weiss KH, Kaler SG (2015) Wilson's disease and other neurological copper disorders. Lancet Neurol 14:103–113. https://doi.org/10.1016/S1474-4422(14)70190-5

[56] Liu J, Simms M, Song S, King RS, Cobb GP (2018) Physiological effects of copper oxide nanoparticles and arsenic on the growth and life cycle of rice (Oryza sativa japonica 'Koshihikari'). Environ Sci Technol 52:13728–13737. https://doi.org/10.1021/acs.est.8b03731

[57] Chan Y-H, Jin Y, Wu C, Chiu DT (2011) Copper(ii) and iron(ii) ion sensing with semiconducting polymer dots. Chem Commun 47(10):2820–2822. https://doi.org/10.1039/C0CC04929H

[58] Gao J, Yin J, Tao Z, Liu Y, Lin X, Deng J, Wang S (2018) An ultrasensitive fluorescence sensor with simple operation for Cu^{2+} specific detection in drinking water. ACS Omega 3:3045–3050. https://doi.org/10.1021/acsomega.7b01497

[59] Xu X, Daniel WL, Wei W, Mirkin CA (2010) Colorimetric Cu^{2+} detection using DNA-modified gold-nanoparticle aggregates as probes and click chemistry. Small 6(5):623–626. https://doi.org/10.1002/smll.200901691

[60] Liu X, Zong C, Lu L (2012) Fluorescent silver nanoclusters for user-friendly detection of Cu^{2+} on a paper platform. Analyst 137(10):2406–2414. https://doi.org/10.1039/C2AN35051C

[61] Mehta VN, Kumar MA, Kailasa SK (2013) Colorimetric detection of copper in water samples using dopamine dithiocarbamate-functionalized Au nanoparticles. Ind Eng Chem Res 52(12):4414–4420. https://doi.org/10.1021/ie302651f

[62] Huang GG, Yang J (2003) Selective detection of copper ions in aqueous solution based on an evanescent wave infrared absorption spectroscopic method. Anal Chem 75(10):2262–2269. https://doi.org/10.1021/ac0264372